Catalysis Science & Technology

Accepted Manuscript

ROYAL SOCIETY OF CHEMISTRY

rsc.li/catalysis

View Article Online
DOI: 10.1039/C7CY02309J

Journal Name

ARTICLE

Understanding the oxidative dehydrogenation of ethyl lactate to ethyl pyruvate over vanadia/titania catalysts

Received 00th January 20xx,
Accepted 00th January 20xx

DOI: 10.1039/x0xx00000x

www.rsc.org/

Wei Zhang,[a] Giada Innocenti,[b] Marilena Ferbinteanu,[c] Enrique V. Ramos-Fernandez,[d] Antonio Sepulveda-Escribano,[d] Haihong Wu,[e] Fabrizio Cavani,[b] Gadi Rothenberg[a] and N. Raveendran Shiju*[a]

We study the vapour-phase oxidative dehydrogenation (ODH) of ethyl lactate with air to give ethyl pyruvate over V_2O_5/TiO_2 catalysts in a fixed-bed reactor. The nature of the vanadia species is changed by varying the vanadium surface density, and the corresponding structure of the VO_x species were determined by XRD, UV-Vis, XPS and H_2-TPR. Monomeric and isolated vanadia species dominate at lower vanadium surface densities. As the surface density increases, two-dimensional polyvanadates and bulk-like vanadia crystallites become predominant. The activity per vanadium decreases with increasing vanadium surface density, indicating that the monomeric VO_x species is better for pyruvate production and that the V–O–Ti bonds play an important role in the ODH of ethyl lactate. This is also confirmed by the superior catalytic performance of V_2O_5/TiO_2 compared to vanadium supported on MgO, Al_2O_3, ZrO_2 and CeO_2. *In situ* DRIFT spectroscopy coupled with a mass analysis shows that the reaction can involve three possible adsorption modes of ethyl lactate on the V_2O_5/TiO_2 surface. Under anaerobic conditions, 2–hydroxypropionate forms, giving ethyl acetate as the major product. Conversely, under aerobic conditions, oxygen that is chemisorbed on V_2O_5/TiO_2 is active and easily replenished from the gas phase, converting the ethyl–propionate–2–oxide intermediate to ethyl pyruvate.

Introduction

Lignocellulosic biomass is one of the few sources of truly renewable carbon.[1-2] But there's a lot of it: even today, the world biomass production could meet the entire carbon demand of the chemical industry (excluding transportation fuels). Typically, biomass is first converted to simple derivatives, or 'platform molecules', that are then reacted further to industrial chemicals. Lactic acid (LA) and lactic esters are important platform molecules. They can be converted to a variety of bulk chemicals, including acrylic acid, propionic acid, pyruvic acid and acetaldehyde.[3-4]

The oxidative dehydrogenation (ODH) of lactic acid to pyruvic acid is especially interesting due to the high demand for pyruvates in the pharmaceutical and agrochemical sectors.[5] Today, pyruvates are still made via the classic dehydrative decarboxylation of tartaric acid in the presence of an excess of $KHSO_4$.[6-7] However, the extra reagent and the high temperature (300 °C) make this process unsustainable. Therefore, attention has focused on oxidative dehydrogenation of lactate as a 'greener' alternative.[8] Several catalysts including Pd/Pt, [9] iron phosphates, [10] metal oxides (Mo, Ti, Zr, W and Sn), [11] and binary oxides (TeO_2–MoO_3, SnO_2–MoO_3)[12-13] were reported for this reaction in both gas phase and liquid phase. Yet most of these also catalyse C–C

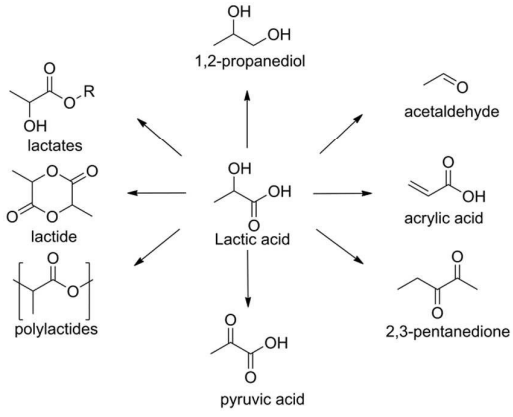

Scheme 1. Lactic acid can be converted to a variety of important bulk chemicals.

[a] Van't Hoff Institute for Molecular Sciences, University of Amsterdam, P.O. Box 94157, 1090GD Amsterdam, The Netherlands. E-mail: n.r.shiju@uva.nl; Web: http://hims.uva.nl/hcsc
[b] Dipartimento di Chimica Industriale, ALMA MATER STUDIORUM Università di Bologna, Viale Risorgimento 4, 40136 Bologna, Italy.
[c] Faculty of Chemistry, Inorganic Chemistry Department, University of Bucharest, Dumbrava Rosie 23, Bucharest 020462, Romania.
[d] Laboratorio de Materiales Avanzados, Departamento de Química Inorgánica-Instituto Universitario de Materiales, Universidad de Alicante, Ctra. San Vicente-Alicante s/n, E-03690 San Vicente del Raspeig, Spain.
[e] Shanghai Key Laboratory of Green Chemistry and Chemical Processes, Department of Chemistry, East China Normal University, 3663 North Zhongshan Road, Shanghai, 200062, China.
Electronic Supplementary Information (ESI) available: [details of any supplementary information available should be included here]. See DOI: 10.1039/x0xx00000x

View Article Online
DOI: 10.1039/C7CY02309J

scission, especially in the gas phase, giving acetaldehyde, CO and CO_2.[5] The catalytic challenge, therefore, is running a selective ODH reaction at a lower temperature, thus avoiding C–C bond scission.Supported/bulk vanadium oxides are used in a variety of ODH reactions at relatively low temperatures.[14-15] The performance of supported vanadium catalysts depends on the type of support and the structure of the surface vanadium species.[16] Compared with other oxide supports, titania interacts strongly with vanadia. The anatase phase in particular gives a stable VOx monolayer with a catalytic oxidation performance superior to that of rutile.[17-18] We recently showed that TiO_2 itself can also catalyse the ODH of ethyl lactate to ethyl pyruvate in the liquid phase, due to its high affinity to ethyl lactate and oxygen.[19] Elsewhere, Li *et al.* reported that $MoVNbO_x$ supported on TiO_2 was more active than unsupported components for vapour phase ethyl lactate conversion.[20] Cavani and co–workers elucidated the role of the components in MoV(Nb)TeO catalysts, showing that vanadium is crucial for achieving high ODH performance.[21] Our preliminary tests showed that commercial V_2O_5 gave higher yields of pyruvate compared with other oxides (MoO_3, V_2O_5, TeO_2 and $MoVO_x$) at low temperatures (Fig. S1). Thus, we hypothesised that VO_x/TiO_2 would be both active and selective in the ODH of lactates.

Here, we studied structure-activity relationships in ethyl lactate ODH over V_2O_5/TiO_2 catalysts. We prepared a series of vanadium oxides supported on anatase TiO_2, varying the vanadium loading via incipient wetness impregnation. Catalyst characterisation showed that different types of VO_x species (monomeric, polymeric, and crystalline domains) formed on TiO_2 surface. We then examined the correlation between VO_x structure and catalytic activity in the ODH of ethyl lactate with air in a fixed-bed reactor, comparing the catalytic properties of V_2O_5 impregnated on TiO_2, MgO, Al_2O_3, ZrO_2 and CeO_2. Across this series, V_2O_5/TiO_2 showed a superior ODH activity, which we attribute to the cooperative effects between vanadia and titania. In situ DRIFT spectroscopy showed that three adsorption modes of ethyl lactate are possible on the V_2O_5/TiO_2 surface. Under anaerobic conditions, 2–hydroxypropionate forms, giving ethyl acetate as the major product. Under aerobic conditions, oxygen chemisorbed on V_2O_5/TiO_2 is active and easily replenished from the gas phase, converting the ethyl–propionate–2–oxide intermediate to ethyl pyruvate.

Results and discussion

Synthesis and characterization of VO_x/TiO_2 catalysts

First, we prepared five supported vanadium oxide catalysts by incipient wetness impregnation using aqueous solutions of ammonium metavanadate (NH_4VO_3) and oxalic acid, which were subsequently dried and calcined at 550 °C. The samples are denoted as *n*–V_2O_5/TiO_2, where *n* represents the wt. % of V_2O_5 on TiO_2 (*n*=1%, 3%, 5%, 10%, 20%; see the experimental section for details).

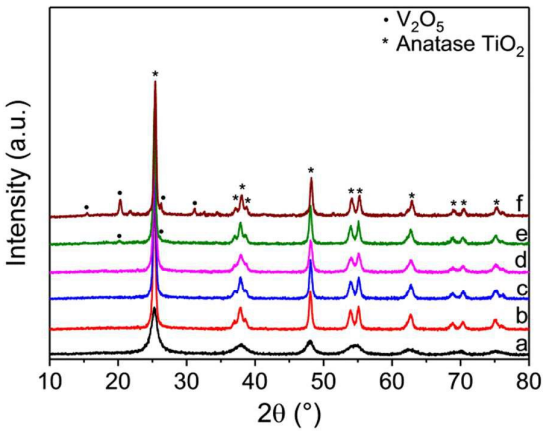

Fig. 1 X-ray diffraction patterns of VO_x/TiO_2 catalysts with different loadings of V_2O_5, (a) pristine TiO_2, (b) 1–V_2O_5/TiO_2, (c) 3–V_2O_5/TiO_2, (d) 5–V_2O_5/TiO_2, (e) 10– V_2O_5/TiO_2 and (f) 20–V_2O_5/TiO_2.

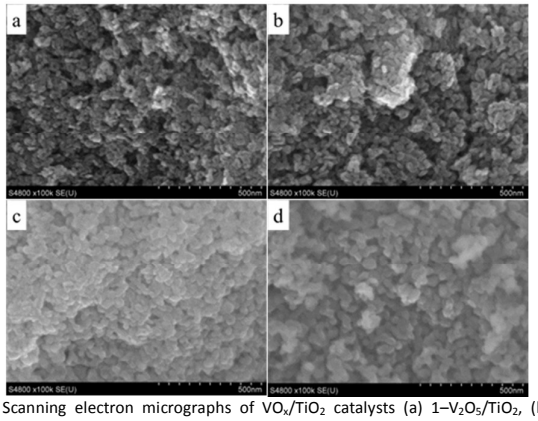

Fig. 2 Scanning electron micrographs of VO_x/TiO_2 catalysts (a) 1–V_2O_5/TiO_2, (b) 3–V_2O_5/TiO_2, (c) 5–V_2O_5/TiO_2, (d) 10–V_2O_5/TiO_2.

Fig. 1 shows the X-ray diffraction (XRD) patterns of the five catalysts. The crystalline structure of anatase TiO_2 remains stable after impregnation with vanadium oxide. No vanadia peaks are detected as the V_2O_5 / (V_2O_5 + TiO_2) ratio increases from 1% to 5%. This suggests that amorphous vanadia species are well dispersed on the TiO_2 surface. When the V loading is increased to 10% and 20%, the peaks of crystalline V_2O_5 can be seen at 20.3° and 26.2°. This probably comes from polymeric vanadia species on the surface.[22] Examining the surface morphology of VO_x/TiO_2 by scanning electron microscopy (SEM) upheld the XRD results (Fig. 2). All samples showed misshaped agglomerated granules, and an increase in particle size with increasing vanadium content. The 20% loaded sample was hereafter discarded, because it contained essentially a separated V_2O_5 phase.

We then studied the textural properties of the catalysts using nitrogen adsorption-desorption isotherms. All samples showed a type IV isotherm with an H1-type hysteresis loop characteristic of mesoporous materials (Fig. 3). As expected, increasing the V content lowered the BET surface area, from 81 m^2/g to 51 m^2/g (Table 1). Actually, the structure of surface VO_x species depends closely on the vanadium surface density (V_{atoms}/nm^2). The surface densities of our samples are 0.8, 3.0,

View Article Online
DOI: 10.1039/C7CY02309J
Journal Name ARTICLE

4.8 and 12.8 V_{atoms}/nm^2, corresponding to V_2O_5 content of 1, 3, 5 and 10 wt%, respectively. The theoretical surface density value for monovanadate is 2~3 V_{atoms}/nm^2. [15] Thus, the vanadia species of 1–V_2O_5/TiO_2 and 3–V_2O_5/TiO_2 are probably isolated VO_4 species, while 5–V_2O_5/TiO_2 and 10–V_2O_5/TiO_2 are predominantly polymeric VO_4 species and V_2O_5 crystallites.[23-24]

b

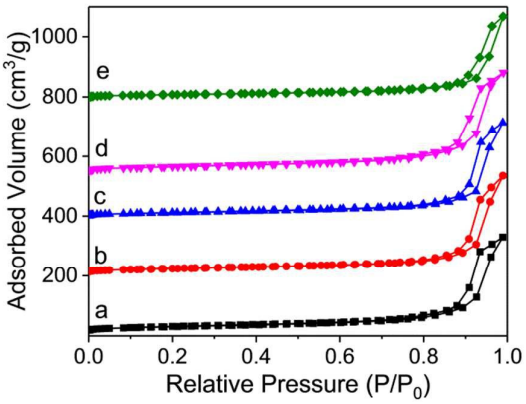

Fig. 3 The Nitrogen adsorption–desorption isotherms of VO_x/TiO_2 catalysts. (a) pristine TiO_2, (b) 1–V_2O_5/TiO_2, (c) 3–V_2O_5/TiO_2, (d) 5–V_2O_5/TiO_2, (e) 10–V_2O_5/TiO_2. The isotherms in the figure are shifted up for the sake of clarity.

Table 1 Textural properties of VO_x/TiO_2 catalysts

Sample	V content [a] (ICP, wt. %)	V surface density (VO_x/nm^2)	S_{BET} [b] ($m^2 g^{-1}$)	V_P [b] ($cm^3 g^{-1}$)
pure TiO_2	–	–	81.3	0.50
1–V_2O_5/TiO_2	0.58	0.8	81.2	0.52
3–V_2O_5/TiO_2	1.80	3.0	70.9	0.51
5–V_2O_5/TiO_2	2.70	4.8	66.3	0.49
10–V_2O_5/TiO_2	5.64	12.8	51.8	0.43

[a] Determined by ICP analysis. [b] Calculated based on N_2 sorption at 77 K.

To confirm the coordination environment of the vanadium species, we used UV–visible diffuse reflectance spectroscopy (UV–vis DRS, see Fig. 4A). The absorption intensity in the visible region is enhanced after depositing vanadium oxide on the titania support. The 1–V_2O_5/TiO_2 showed charge-transfer bands centred around 280–350 nm, assigned to isolated tetrahedral V^{5+} species.[25] As V_2O_5 loading increased, the absorption bands shifted to higher wavelengths, reflecting the lower-energy transitions of the charge transfer between oxygen and V atoms.[26] This indicates the formation of highly coordinated polymeric vanadium species from isolated tetrahedral monomeric species (*cf.* the similar structures observed for molybdenum [27]). Increasing the vanadia content to 10 wt% showed crystalline V_2O_5 species (absorption at 490 nm [28-29]). Defining the position of isolated and polymerized VO_4 units using UV−vis DRS is difficult, as their absorption bands can overlap with the strong absorption of the titania support.[30] However, the absorption edge energy (E_g) can give quantitative information of coordination number and the local structure of VO_x species. The E_g is determined by finding the intercept on the X-axis of the tangent line in the low-energy rise of the plot of $[F(R_\infty)h\nu]^2$ *vs.* $h\nu$, where $F(R_\infty)$ is the Kubelka-Munk function and $h\nu$ is the incident photon energy.[31] The corresponding E_g values for V_2O_5/TiO_2 are shown in Fig. 4B, wherein the value of pure TiO_2 is about 3.27 eV. For the V_2O_5/TiO_2 catalysts, the E_g value gradually decreases with increasing surface vanadia content, from 3.19 to 2.1 eV. A similar trend was observed by Danilevitch *et al*.[32] The high E_g value at low vanadium surface density corresponds to isolated surface VO_4 species. When the vanadium content is 1%, E_g≈3.19 eV, which is close to the value of 3.21 eV for Na_3VO_4 (where vanadium exists as an isolated tetrahedral VO_4 species).[33] Bulk $NaVO_3$ was reported to have a polymeric tetrahedral VO_4 structure with an E_g value of 2.41 eV.[34] Thus, we assume that the 3% V_2O_5 on TiO_2 (with E_g=2.84 eV) contains also polymerized VO_4 units in addition to isolated VO_4 species. Increasing the V_2O_5 content to 5% yielded an E_g value of 2.38 eV, indicating the presence of a higher amount of polyvanadate species. Note that the E_g value of 10% V_2O_5/TiO_2 (2.10 eV) is close to that of bulk V_2O_5 (2.05 eV),[15] suggesting that the polymerized VO_4 species is aggregated to crystalline V_2O_5, in agreement with the XRD results.

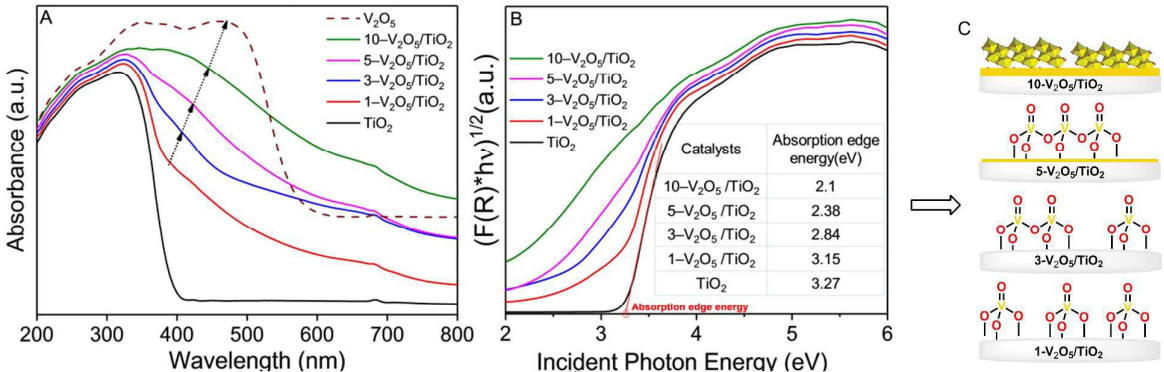

Fig. 4 (A) UV–Vis absorption spectra of TiO_2, V_2O_5 and V_2O_5/TiO_2 catalysts, (B) $[F(R\alpha)h\nu]^{1/2}$ plotted against the energy of the incident photon for the determination of edge energy for V_2O_5/TiO_2 catalysts; the inset shows the corresponding E_g values. The edge energies are determined from the intercept on the X-axis of a straight line fitted through the rise of the function $[F(R\alpha)h\nu]$ (C) Schematic structures of V_2O_5/TiO_2 catalysts showing different type of vanadia species.

View Article Online
DOI: 10.1039/C7CY02309J

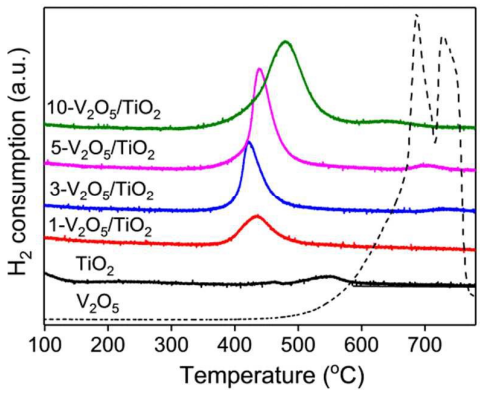

Fig. 5 H_2-TPR profiles of the TiO_2, V_2O_5 and V_2O_5/TiO_2 catalysts.

We ran H_2–TPR experiments to further elucidate the oxidation state of surface vanadia species and the reducibility of V_2O_5/TiO_2 catalysts (see Fig. 5).[35] The pristine TiO_2 support showed only a very weak peak around 540 °C. After depositing vanadia, the temperature of the maximum hydrogen consumption (T_{max}) shifted lower, also compared with pure V_2O_5. This suggests that V_2O_5/TiO_2 is easier to reduce than pure TiO_2 or V_2O_5. Among our V_2O_5/TiO_2 catalysts, the T_{max} shifted to higher temperature with increasing V_2O_5 content. Generally, the reducibility of supported V_2O_5 catalysts is affected both by the type of surface vanadia species and vanadium coverage. Indeed, polymeric VO_x species in the monolayer are reported as more easily reduced than monomeric ones. [36-37] In our case, the 3–V_2O_5/TiO_2 sample, which contains also polymerized VO_4 units, was more easily reduced compared to the 1–V_2O_5/TiO_2 sample (which has only monomeric VO_4 species, in agreement with published data [38]). VO_x species below or at monolayer coverage are more reducible than the VOx species in multilayers and in crystalline or bulk vanadia. Accordingly, reducing the 5–V_2O_5/TiO_2 and 10–V_2O_5/TiO_2 was even more difficult, in agreement with this trend.[39-40]

We then ran X-ray photoelectron spectroscopy (XPS) measurements to identify the chemical species on the surface (see Fig. 6). The V 2 $p_{3/2}$ peak (Fig. 6a) was deconvoluted into two distinct peaks centered at 516.5 eV and 517.5 eV, corresponding to V^{4+} and V^{5+} species, respectively.[17] The peaks at 464.7 eV and 458.9 eV are assigned to the Ti 2 $p_{1/2}$ and Ti 2 $p_{3/2}$ (Fig. 6b), suggesting that the Ti^{4+} state predominates.[41] Similarly, the spectra of O 1*s* (Fig. 6c) were fitted with three peaks. The main peak was observed at a lower BE of 530.2 eV, and assigned to lattice oxygen species (O_β). The peak at around 531.7 eV represented the surface chemisorbed oxygen (O_α), while that at 532.6 eV represented the chemisorbed water (O_α').[34, 42]

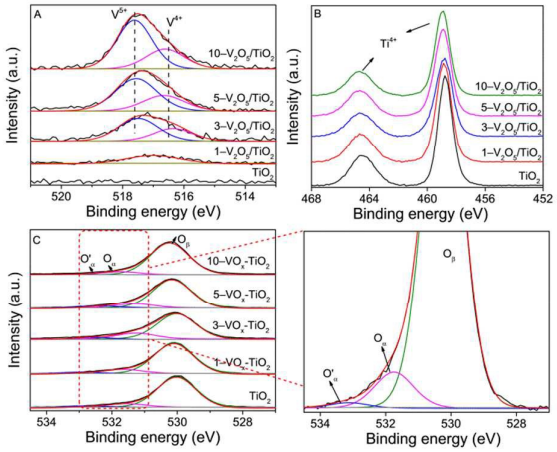

Fig. 6 XPS spectra of the V_2O_5/TiO_2: (A) high resolution V_{2p} spectra, (B) high resolution Ti_{2p} spectra and (C) high resolution O_{1s} spectrum.

Catalytic activity

We first analysed the mass-transfer limitations for the oxidative dehydrogenation of ethyl lactate with air over 3–V_2O_5/TiO_2 catalysts in a fixed-bed reactor. For studying intra-particle diffusion limitation, we ran a series of experiments varying the catalyst particle sizes from 20 to 80 mesh. As shown in Figure S2, the ethyl lactate conversion remained constant, ruling out the internal diffusion limitations. The external diffusion limitation was also examined by changing the ethyl lactate feed rate and the catalyst amount. Here we varied the catalyst amount (W) as 0.5 g, 1 g, 1.5 g and 2g (Figure S3) and for each catalyst weight, we changed the flow rates (F). The ethyl lactate conversion plotted against W/F (Figure S3) shows that the curves are similar, indicating the absence of external diffusion limitations.[43]

Then we studied the effect of reaction temperature on the ODH of ethyl lactate over 3–V_2O_5/TiO_2 (Figure S4). Ethyl lactate conversion increased from 60% to 95% when the reaction temperature was raised from 160 °C to 340 °C. High temperature facilitated the undesired side reactions. The optimal temperature is about 180 °C, which gave the highest pyruvate selectivity of 80%. Figure S4 also shows the change in product selectivity at different temperatures. At low temperature (below 200 °C), ethanol was the main by-product due to the hydrolysis of ethyl lactate. Minor by-products such as acetaldehyde and acetic acid were also detected. Additionally, acrylate (acrylic acid and ethyl acrylate) and propionate (propionic acid/ethyl propionate) were formed with rising temperature, reaching selectivity of 15% and 18% respectively at 340 °C. This indicates that dehydrogenation and dehydration occur at high temperatures, in line with previous reports.[44]

We also varied Liquid Hourly Space Velocity (LHSV) of ethyl lactate from 0.5 h^{-1} to 3.5 h^{-1} (corresponding to 1–8 ml/h ethyl lactate feeding rate), and the results are summarized in Table S1. As expected, with an increase in the LHSV, the ethyl lactate conversion gradually decreased due to the decrease in

View Article Online
DOI: 10.1039/C7CY02309J

contact time. The ethyl pyruvate selectivity increased from 20% to 80% with the change in LHSV from 0.5 to 2.5 h^{-1}. However, further increase in LHSV did not favor pyruvate. This is probably due to the coverage of the active sites of the catalyst by reactant leading to coke formation.

Then, the activities of V_2O_5/TiO_2 catalysts for the ODH reaction of ethyl lactate to ethyl pyruvate were investigated. Pure anatase TiO_2 support gave only low yield. Similarly, control experiments with commercial bulk V_2O_5 gave <30% of pyruvate. Interestingly, even 1–V_2O_5/TiO_2 gave higher selectivity and yield than bulk V_2O_5 (Figure 7). Note that the specific surface area of 1–V_2O_5/TiO_2 is 81 m^2/g, much higher than that of V_2O_5 (5 m^2/g). This suggests that highly dispersed vanadia is responsible for the catalytic activity. When the vanadium loading increased to 3%, the selectivity to pyruvate reached a maximum of 78% at 62% conversion. Increasing the V loading further did not improve the catalytic performance. To differentiate better the influence of surface vanadia species on catalytic performance, control experiments were performed by increasing LHSV and decreasing air flow at low reaction temperature (160 °C, 180 °C vs. 200 °C). Figure 8 shows that all V_2O_5/TiO_2 catalysts show higher ethyl lactate conversion than pure TiO_2 and V_2O_5. Sub-monolayer 1–V_2O_5/TiO_2 catalyst gave 10% ethyl lactate conversion at 160 °C. Increasing vanadia loading to 3% (near monolayer coverage) gave an ethyl lactate conversion of 28%. With vanadia content over 3%, the conversion almost levelled-up. We therefore attribute the reactivity enhancement to non-polymeric vanadium species close to TiO_2.[45]

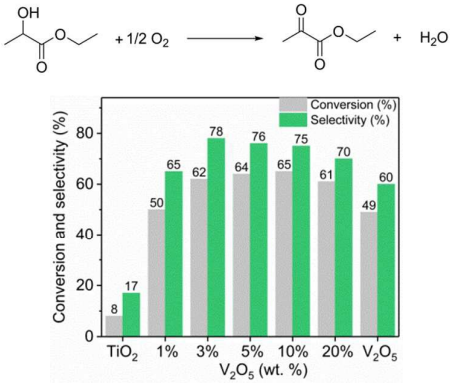

Fig. 7. The effect of V_2O_5 loading on ethyl lactate conversion and ethyl pyruvate selectivity over V_2O_5/TiO_2 catalysts. Reaction conditions: 5 ml/h Ethyl lactate, 2.25 L/h air flow (molar ratio of ethyl lactate/O_2=2.3), 1.0 g catalyst, 200 °C.

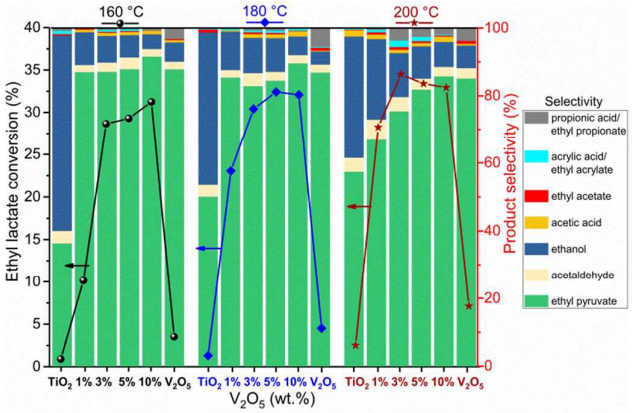

Fig. 8 The effect of V_2O_5 loading on ethyl lactate conversion and ethyl pyruvate selectivity over V_2O_5/TiO_2 catalysts. Reaction conditions: 8 ml/h Ethyl lactate, 1 L/h air flow (molar ratio of ethyl lactate/O_2=5), 1.0 g catalyst, Reaction temperature: 160 °C 180 °C and 200 °C.

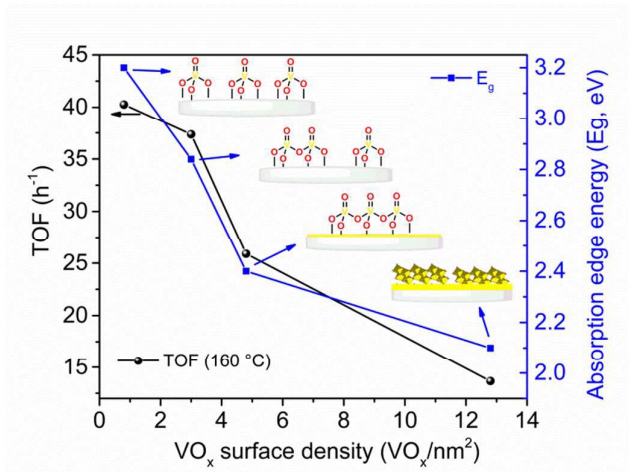

Fig. 9 Relationship between TOF of ethyl lactate oxidation, absorption edge energy (E_g) and VO_x surface density of VO_x/TiO_2 catalysts. Reaction conditions: 10 ml/h Ethyl lactate, 1 L/h air flow (molar ratio of ethyl lactate/O_2=5), 1.0 g catalyst, 160 °C.

To further evaluate the catalytic performance of V_2O_5/TiO_2, we calculated the turnover frequency (TOF) under relatively low conversion of ethyl lactate and shown in Fig. 9. The TOF of V_2O_5/TiO_2 was inversely proportional to the vanadium surface density, in close correlation with the absorption edge energy (E_g, see the right axis in Fig. 9). The low V surface density with high E_g, where the vanadium is present as monomeric species, gave the highest TOF. As VO_x surface density increases, isolated VO_4 species agglomerate with their nearest neighbours, resulting in a lower ratio of V–O–Ti bonds and an increase in V–O–V and V=O bonds. Meanwhile, the V–O–Ti bonds within multilayer are less accessible than those in the surface monolayer,[46] which may explain the lower selectivity at higher vanadium loadings. Ji *et al* reported that the ratios of $V^{4+}/(V^{4+}+V^{5+})$ reflected the ratio [(vanadium stronglyinteracting with the support)/(total vanadium)],[24] in our case, the V loading increased from 1% to 10%, the ratios of $V^{4+}/(V^{4+}+V^{5+})$ decreased from 0.5 to 0.29 (Table S2). This result confirms the decrease in V–O–Ti bonds. Earlier Wachs *et al.* showed that

View Article Online
DOI: 10.1039/C7CY02309J

the reactivity of VO_x species is unrelated to the terminal V=O bonds in partial oxidation of methanol.[47] Oxygen labelling experiments also demonstrated that the V=O bond is stable during butane oxidation.[48-49] In our system, the terminal V=O bonds do not favour the TOF of ethyl lactate conversion, this will be proved by our latter DRIFTS Study. The fact that the 1–V_2O_5/TiO_2 catalyst, which has negligible V–O–V bonds, gave comparable catalytic activity, confirms that the bridging V–O–V bond does not play a role in our reaction.[47] For comparison, we prepared a mixture of V_2O_5 and TiO_2 by mixing bulk V_2O_5 and TiO_2 powder in a mortar. This physical mixture, which contained 3 wt. % V_2O_5, gave only 5.6% yield of ethyl pyruvate, compared to the 48.1% yield obtained over impregnated V_2O_5/TiO_2 (with the same vanadium loading and at otherwise identical reaction conditions). Thus, we concluded that the catalytic performance is determined by the structure of surface vanadium species, and especially the V–O–Ti bonds play a critical role in the oxidative dehydrogenation of ethyl lactate.

Table 2 ODH of ethyl lactate to ethyl pyruvate over V_2O_5 on various supports.[a]

Entry	Catalyst	S_{BET} ($m^2\ g^{-1}$) [b]	Con. (%) [c]	Sel. (%)	Yield (%) [c]	Surface PH [d]
1	1–V_2O_5/CeO_2	50	1	32.2	trace	6.75
2	1–V_2O_5/MgO	198	15.9	0.5	trace	11
3	1–V_2O_5/ZrO_2	89	28.5	43.9	12.5	5.9-6.1
4	1–V_2O_5/Al_2O_3	278	35.6	36.7	13.1	8.9
5	1–V_2O_5/TiO_2	81	58.7	63.7	37.4	6.0-6.4

[a] Reaction conditions: 5 ml/h Ethyl lactate, 2.25 L/h air flow (molar ratio of ethyl lactate/O_2=2.3), 1.0 g catalyst (1 wt. % of metal oxide on TiO_2), 180 °C. [b] Calculated based on N_2 sorption at 77 K. [c] Determined by GC using biphenyl as an external standard. [d] Based on ref.[50] and [51].

Three types of bonds can be present in supported vanadia catalysts: V=O, V–O–V and V–O–M (where M is the support metal cation). To understand the importance of the V–O–M bonds, we studied vanadium oxide catalysts supported on four different supports: MgO, Al_2O_3, ZrO_2 and CeO_2, varying the support surface acidity.[50] For a fair comparison of V=O and V–O–V bonds, we prepared porous supports with high surface area and subsequently impregnated 1 wt.% of vanadium oxide on each support to form isolated VO_x species (see the experimental section for details). The acidity of oxide supports is a key factor in many ODH systems.[52] The relative acidity in this series is Al_2O_3> TiO_2> ZrO_2> CeO_2> MgO.[53-54] In each case, we first tested the support alone in our reaction at 180 °C. Only MgO showed some conversion (13%), but no selectivity (because ethyl lactate undergoes hydrolysis to ethanol and lactic acid on the basic MgO surface). After introducing vanadia, the catalytic activities of those supported vanadia catalysts are summarized in Table 2. After impregnation, the reactivity of V_2O_5/MgO was unchanged. Conversely, the catalyst supported on acidic Al_2O_3 showed high conversion, but with low selectivity, owing to a competing decarboxylation of ethyl pyruvate to acetaldehyde.[13] TiO_2–supported vanadium oxide showed the highest catalytic activity, while V_2O_5/ZrO_2 and V_2O_5/CeO_2 scarcely catalyze the reaction under identical conditions. Fig. 10 shows the Arrhenius plots of ethyl lactate consumption rates. For 1–V_2O_5/TiO_2, the apparent activation energy (Ea) of ethyl lactate conversion (48 kJ/mol) is lower than that of 1–V_2O_5/Al_2O_3 (57 kJ/mol), 1–V_2O_5/ZrO_2 (75 kJ/mol) and 1–V_2O_5/CeO_2 (127 kJ/mol). These results confirmed that the monomeric V–O–Ti species is more catalytically active, confirming further the importance of the vanadium–oxygen interactions.

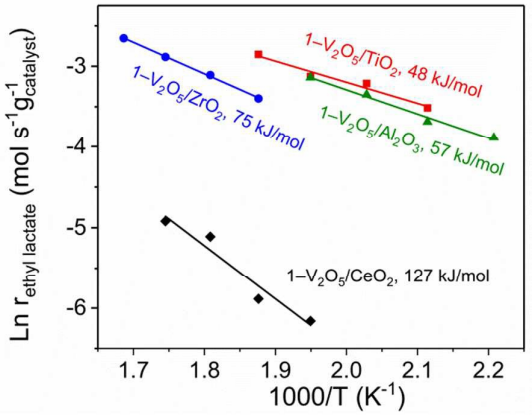

Fig. 10 Arrhenius plots for steady-state ethyl lactate conversion over supported V_2O_5 catalysts. Reaction conditions: LHSV= 4 h^{-1}, air flow= 1 L/h. Ethyl lactate consumption rate: $r_{ethyl\ lactate} = \frac{\text{moles of ethyl lacate per hour in the reactor (mol/s)}}{\text{mass of catalyst (g)}}$. The apparent activation energy (Ea) was measured at a series of temperatures under 20 % ethyl lactate conversion.

***In situ* DRIFTS Study.** Further insight into the reaction can be gained by *in situ* diffuse reflectance infrared Fourier transform spectroscopy (DRIFTS). Fig. 11 shows the *in situ* DRIFTS of temperature-programmed ethyl lactate desorption on 3–V_2O_5/TiO_2 in the absence of oxygen. The characteristic bands of ethyl lactate adsorbed on V_2O_5/TiO_2 were detected. The C–H vibrations were observed at 2990 cm^{-1}, 2940 cm^{-1}, 2883 cm^{-1}, 1454 cm^{-1}, 1387 cm^{-1} and 1302 cm^{-1}, and ascribed to $\nu_s(CH_3)$, ν (C–H), $\delta_{as}(CH_3)$, $\delta_s(CH_3)$ and δ (C–H), respectively.[55-56] Those bands decreased in intensity with rising temperature, indicating the degradation of ethyl lactate.[57] This process was also reflected by the changes of the carbonyl and carboxyl on the V_2O_5/TiO_2 surface (four peaks at 1730 cm^{-1},1667 cm^{-1}, 1566 cm^{-1} and 1420 cm^{-1}, assigned to ν (C=O), ν (C=O···M^+), ν_s (COO) and ν_{as} (COO) vibrations, respectively).[55, 58-59] Increasing the temperature broadens those carbonyl and carboxyl peaks, where the signals of ν_s (COO) and ν_{as} (COO) were blue shifted to 1540 cm^{-1} and 1445 cm^{-1} over 250 °C. This is because of the formation of adsorbed acetate species.[60] Evidently, we detected the ethyl acetate by monitoring the mass signals during the temperature-programmed ethyl lactate desorption (Fig. S6). The C=O stretching of ethyl lactate was weakened (1730 cm^{-1} and 1667 cm^{-1}), accompanying two new shoulder peaks at 1780 cm^{-1} and 1651 cm^{-1}. These bands were assigned

View Article Online
DOI: 10.1039/C7CY02309J

to the carbonyl stretching of the α-keto group of the pyruvate,[57] supporting the experimental results (Fig. S5), the surface chemisorbed oxygen of V_2O_5/TiO_2 could participate in the oxidation of lactate without molecular oxygen. the surface chemisorbed oxygen of V_2O_5/TiO_2 could participate in the oxidation of lactate without molecular oxygen. The bands at 1224 cm^{-1} and 1141 cm^{-1} may reflect the alcohol OH related C–O stretching vibrations of ethyl lactate.[61]

Analysing the DRIFT spectra shows several possible adsorption modes of ethyl lactate on catalyst surface (Table 3). The main features are the vibration differences of C–O, carbonyl (C=O) and carboxyl(COO) groups. The three adsorption modes (a), (b) and (c) were detected in line with published data,[55] while

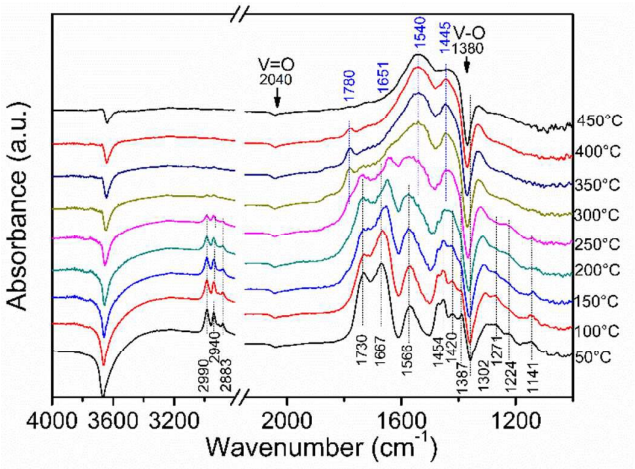

Fig. 11 *In situ* DRIFT spectra recorded during ethyl lactate temperature-programmed-desorption over 3–V_2O_5/TiO_2 with He flow (without O_2).

Table 3. Ethyl lactate adsorption modes and their vibration wavenumber.

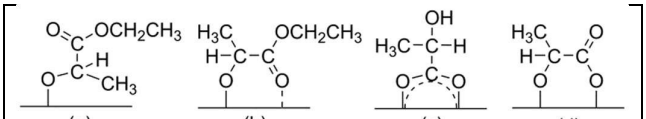

Molecules	Vibrational mode	Wavenumber (cm^{-1})[a]	Wavenumber (cm^{-1})[b]
	v (C=O)	1725	1730
	δ_{AL}(C–O)	1220	1224
	v_s (COO)	1569	1566
	v_{as} (COO)	1421	1420
	v (C=O)	1668	1667
	δ_{AL}(C–O)	1220	1224
	v_s (COO)	1570	1566
	v_{as} (COO)	1450	1420
	v_{AL}(C–O)	1140	1141
	δ_{AL}(OH)	1270	1271
	v (C–O)	1058	Not detected
	v (C–O)	1118	Not detected
	v (C=O)	1614	Not detected

AL = Alcoholic functionalities

[a] Based on ref. [55] and [56]; [b] From our *in situ* DRIFTS.

mode (d) was not detected. The weak band at 1271 cm^{-1} can be attributed to the O–H stretch of mode (c). Considering the model (c) has no carbonyl stretching signals, model (a) and (b) dominate at low temperature. The mass signals of both ethanol and CO_2 increased with temperature (Fig. S6), due to the decomposition process. This agrees well with the changes of *in situ* DRIFTS.

We also studied *in situ* DRIFTS experiments of ethyl lactate adsorbed 3–V_2O_5/TiO_2 with O_2. As shown in Fig. 12, the vibrational bands of ethyl lactate on catalyst were similar to the spectra at low temperatures (*cf.* Fig. 11).

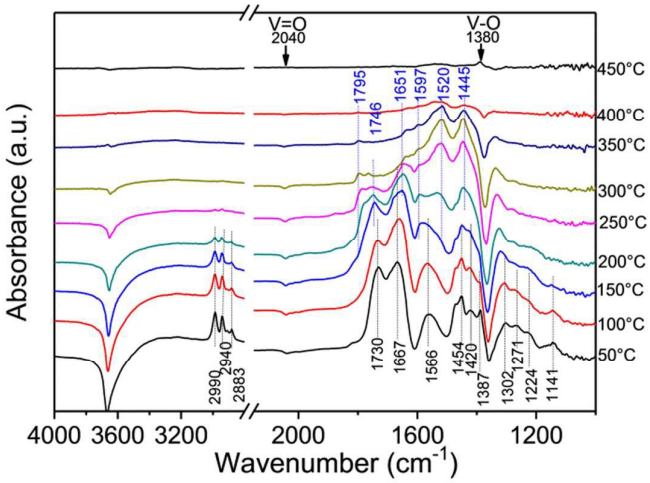

Fig. 12 *In situ* DRIFT spectra recorded during ethyl lactate temperature-programmed-desorption over 3–V_2O_5/TiO_2 with air flow (with O_2).

Upon increasing temperature to 150 °C, we observed the characteristic bands of α-keto in pyruvate (1795 cm^{-1} and 1651 cm^{-1}), [57] together with a red-shifted COO stretch at 1597 cm^{-1}. [55, 62] The *in situ* DRIFTS were also reflected the adsorption and dissociation of ethyl lactate on V_2O_5/TiO_2 surface in the presence of oxygen. Due to the formation of pyruvate species, the position of carbonyl *v* (C=O) were shifted to 1746 cm^{-1}, [62] as compared to the *v* (C=O) of ethyl lactate at 1730 cm^{-1}; The peaks at 1141 cm^{-1} (C–O belongs to model (a) and (b)) also started to weakened at 150 °C, accompanying the characteristic peaks of pyruvate; while the characteristic peaks of model (c) were unchanged. This means that ethyl–propionate–2–oxide (in mode a and b) is the key intermediate to produce pyruvate (similar to the ethoxide species in ethanol oxidation[60-61]). The decrease of the negative peak at 3662 cm^{-1} upheld this dehydration processes. Additionally, the intensity of pyruvate bands decreased as the temperature increased over 250 °C, indicating a decomposition process (Fig. S7). The pyruvate peaks disappeared at 400 °C. Meanwhile, the new bands at 1520 cm^{-1} and 1445 cm^{-1} were attributed to surface

View Article Online
DOI: 10.1039/C7CY02309J

carbonates ν_{as}(COO) and ν_{s}(COO),[63] as pyruvate is easily over-oxidised to form the carbonates as side products.[64]

The bands at 2040 cm^{-1} and 1380 cm^{-1} are attributed to the V=O bond overtone band and the V–O bond combination band (probably belonging to V–O–Ti), respectively (for a detailed analysis of the pristine V_2O_5/TiO_2 see Fig. S8).[61] The presence of negative bands means that VO_x interacts with the adsorbed species. Under anaerobic condition (Fig. 11), the V=O stretch remained constant with temperature, while the V–O was blue shifted (from 1360 cm^{-1} at 50 °C to 1380 cm^{-1} at 400 °C). In presence of air, the V=O band is well preserved after the formation of pyruvate band, then vanishes at 350 °C along with pyruvate species; while the V–O band, diminished in intensity, is still present at 400 °C in presence of carbonates. These observations support the hypothesis that V=O bonds are not involved in the ODH of ethyl lactate while V–O ones play a key role in the reaction.

In Fig. 13, we propose a reaction network for the aerobic and anaerobic conversion of ethyl lactate. Ethyl lactate first absorbs and dissociates on the V_2O_5/TiO_2 surface, with adsorption modes (a), (b) and (c). Modes (a) and (b) dominate at low temperature, while model (c) generates 2–hydroxypropionate on the surface through a hydrolysis process at higher temperatures. In absence of molecular oxygen, increasing the temperature accelerates the formation of mode (c), subsequently giving ethyl acetate as the major product. Pyruvate species can also be produced, but are limited by the surface chemisorbed oxygen. Under aerobic conditions, however, molecular oxygen reoxidizes the catalyst, replenishing the surface oxygen and promoting the oxidative dehydrogenation of ethyl lactate to ethyl pyruvate.

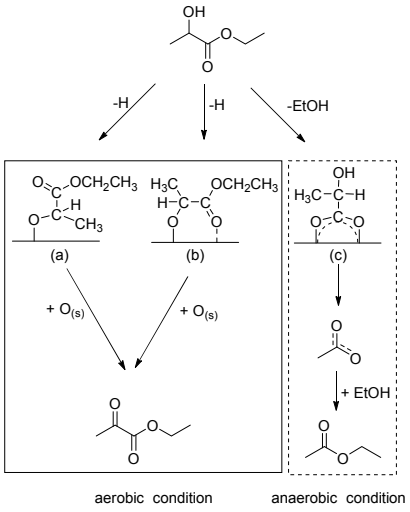

Fig.13 Proposed reaction pathway for the aerobic and anaerobic conversion of ethyl lactate over V_2O_5/TiO_2 catalyst.

Conclusions

We studied the catalytic oxidative dehydrogenation of ethyl lactate to ethyl lactate over V_2O_5/TiO_2 catalysts. To explore the structure-activity relationship for various vanadia species, a series of V_2O_5/TiO_2 with different surface densities were prepared via incipient wetness impregnation. As their surface density increases, the isolated VO_x species agglomerated to polymeric and crystalline VO_x species, leading to a decrease in TOF of ethyl lactate oxidation. The titania-supported vanadium oxide was superior to vanadia catalysts supported on MgO, Al_2O_3, ZrO_2 and CeO_2. This shows that V–O–Ti bonds play a key role in the oxidative dehydrogenation of ethyl lactate to ethyl pyruvate. *In situ* DRIFTS showed that the ethyl–propionate–2–oxide species on catalyst surface are the key intermediates in this reaction via dehydrogenation. Molecular oxygen can replenish the surface oxygen, accelerating the oxidative dehydrogenation of ethyl lactate to ethyl lactate. This work allowed us to understand the chemical-physical features needed for a vanadium-oxide based catalyst in order to be active and selective in the ODH of ethyl lactate to ethyl pyruvate, thus opening new perspectives in the valorisation of bio-based platform molecules.

Experimental Section

Materials and instrumentation.

All chemicals were commercially available and used without further purification: Anatase titania (Hombikat M311), (–)–Ethyl L–lactate (Sigma–Aldrich, ≥98.0%, analytical standard), Ammonium metavanadate (Acros organics, 99.5% analytical standard), Oxalic acid (Sigma–Aldrich, ≥99.0%, analytical standard), Vanadium(V) oxide(Alfa Aesar, 99.2%), Magnesium oxide nanopower (Strem Chemicals, S.A.≥ 230 m^2/g, >95%), Aluminium oxide (Sasol, S.A.=181 m^2/g, 97%), Zirconium(IV) oxide nanopower (Sigma–Aldrich, S.A. ≥25 m^2/g, 99.0%), Cerium(IV) oxide(Alfa Aesar, S.A.=30–50 m^2/g, 99.5%). X–ray diffraction patterns were recorded on a Rigaku Mini Flex II diffractometer instrument using Cu–Kα radiation (λ = 1.5406 Å) at 35 kV and 30 mA. Nitrogen adsorption–desorption isotherms were measured on a Quantachrome Autosorb–3B instrument after evacuating the samples at 523 K for 6 h. The specific surface areas were evaluated using the Brunauer–Emmett–Teller method. The vanadium loading was measured by inductively coupled plasma (ICP) atom emission spectroscopy (AES) on a Thermo IRIS Intrepid II XSP. UV−visible diffuse reflectance spectra were collected on a Jasco V670 spectrophotometer with spectralon as standard in the range 200 – 1000 nm. Scanning electron micrographs were recorded using a Hitachi S–4800 microscope. Temperature programmed reduction (TPR) measurements were performed on a 1100 Series Thermo Electron TPDRO machine by using a stream of 5% H_2/N_2 and a heating rate of 5 °C min^{-1}. XPS spectra were collected using a Thermo Scientific K–ALPHA with Al–K radiation (1486.6eV), monochromatized by a twin crystal monochromator, yielding a focused X–ray spot with a diameter of 400 μm, at 3 mA × 12 kV when charge compensation was achieved with the system flood gun that provides low energy

View Article Online
DOI: 10.1039/C7CY02309J

electrons and low energy argon ions from a single source. The alpha hemispherical analyzer was operated in the constant energy mode with survey scan pass energies of 200 eV to measure the whole energy band and 50 eV in a narrow scan to selectively measure the particular elements. An estimation of the intensities was done after a calculation of each peak integral, S–shaped background subtraction and fitting the experimental curve to a combination of a Lorentzian (30%) and Gaussian (70%) lines. Binding energies (BE), referenced to the C 1s line at 284.6 eV, have an accuracy of ± 0.1 eV. In situ Diffusion reflectance infrared Fourier transform (DRIFT) spectra was recorded using a Bruker Vertex 70 spectrometer equipped with a Pike DiffusIR cell attachment. The cell window was made of ZnSe. Spectra were recorded using a MCT detector after 128 scans and 4 cm^{-1} resolution. The instrument is online with a mass spectrometer EcoSys–P from European Spectrometry Systems. In each experiment the sample was pretreated at 450°C in He for 30 min in order to provide a clean catalyst surface. After, the carrier gas was switched to air in the test in presence of oxygen. This last passage was omitted in the tests in absence of O_2. Then the IR backgrounds were collected every 50 degrees from 450 °C to 50 °C. Afterwards, L–ethyl lactate (EL) pulse was done at 50°C. Then, the catalyst was kept under the carrier gas flow for 30 min in order to eliminate physisorbed molecules. Sample temperature was then increased by 5°C/min and spectra were collected every 50°C. During the overall IR analysis several mass signals (m/z) were monitored continuously: 4, 14, 15, 17, 18, 27, 28, 29, 31, 42, 43, 44, 45, 46, 58, 60, 61, 70, 74, 103, and 116. Conversion and selectivity were quantified on an Agilent 7820A GC equipped with a flame ionization detector (FID) and a dimethylpolysiloxane capillary column (VB–1, 30 m × 0.32 mm × 3.00 μm).

Preparation of V_2O_5/TiO_2

The supported vanadium oxide catalysts were prepared following the procedure reported by Srinivas *et al.*[64] In a typical synthesis of V_2O_5/TiO_2 catalyst, the TiO_2 was impregnated with the aqueous solutions of ammonium metavanadate (NH_4VO_3) and oxalic acid, followed by drying and calcining for 4 h at 550 °C. The resulting solid was denoted as *n*–V_2O_5/TiO_2, where *n* represents the weight percent of V_2O_5 on TiO_2. (*n* =1%, 3%, 5%, 10%, 20%).

Preparation of porous MgO, ZrO_2 and CeO_2

Porous MgO was prepared according to a previous report.[65] 10 grams of magnesium hydroxide carbonate was calcined at 500 °C for 4 hours at a heating rate of 1 °C/min and then cooled to room temperature.

Porous ZrO_2 was prepared following the procedure reported by Davshan *et al.*[66] 7.8 grams of cetyltrimethylammonium bromide (CTMABr) was added to 50 ml water. Then the pH value was adjusted to 2 by adding 2.0 M HCl solution. Next, zirconium propoxide solution (70 wt. % in 1-propanol) was added to the premixed solution under rigorous stirring for 1h. After that, the mixture was transferred into an autoclave and heated at 60 °C for 48 h. Then, the precipitate was filtered off and calcined at 600 °C for 2h under air flow.

Porous CeO_2 was synthesized according to the method described by Li *et al.*[67] Briefly, 5 grams of cerium nitrate hexahydrate ($Ce(NO_3)_3{\cdot}6H_2O$) and 55 grams of NaOH were dissolved in 25 ml H_2O under vigorous stirring for 2h. Then, the mixture was transferred into an autoclave and heated at 180 °C for 24 h. After that, the suspension was filtered, washed with water and dried at 80 °C overnight.

Procedure for catalytic experiments

The oxidative dehydrogenation of ethyl lactate to ethyl pyruvate was carried out in a fixed–bed quartz reactor with internal diameter of 4 mm and length of 300 mm. The catalyst (1g, 20–25 mesh) was placed in the middle of the reactor and the upper part was filled with quartz sands for preheating the ethyl lactate. Ethyl lactate was injected into the reactor at a rate of 5ml/h by a syringe pump and using air as the carrier gas and terminal oxidant. After each reaction period of 2 h, the products were collected in a cold trap and add a calculated amount of biphenyl was added as an external standard for GC analysis.

Conflicts of interest

There are no conflicts to declare.

Acknowledgements

WZ thanks the China Scholarship Council for a PhD fellowship. EVRF thanks Generalitat Valenciana (project PROMETEOII/2014/004), and Ministerio de Economía y Competitividad (Spain) for projects MAT2013-45008-P, MAT2016-81732-ERC and RYC-2012-11427. This work is part of the Research Priority Area Sustainable Chemistry of the UvA, http://suschem.uva.nl.

References

1 A. Corma, S. Iborra and A. Velty, *Chem. Rev.*, 2007, **107**, 2411.
2 P. N. R. Vennestrøm, C. M. Osmundsen, C. H. Christensen and E. Taarning, *Angew. Chem. Int. Ed.*, 2011, **50**, 10502.
3 M. Dusselier, P. Van Wouwe, A. Dewaele, E. Makshina and B. F. Sels, *Energy Environ. Sci.*, 2013, **6**, 1415.
4 R. Beerthuis, G. Rothenberg and N. R. Shiju, *Green Chem.*, 2015, **17**, 1341.
5 P. Mäki-Arvela, I. L. Simakova, T. Salmi and D. Y. Murzin, *Chem. Rev.*, 2014, **114**, 1909.
6 E. Erlenmeyer, *Ber. Dtsch. Chem. Ges.*, 1881, **14**, 320.
7 F. Howard, *Org. Syn. Coll.*, 1941, **1**, 475.
8 F. A. Castillo Martinez, E. M. Balciunas, J. M. Salgado, J. M. Domínguez González, A. Converti

View Article Online
DOI: 10.1039/C7CY02309J

and R. P. d. S. Oliveira, *Trends Food Sci.Technol.*, 2013, **30**, 70.
9 S. Sugiyama, T. Kikumoto, H. Tanaka, K. Nakagawa, K.-I. Sotowa, K. Maehara, Y. Himeno and W. Ninomiya, *Catal. Lett.*, 2009, **131**, 129.
10 M. Ai and K. Ohdan, *J. Mol. Catal. A: Chem.*, 2000, **159**, 19.
11 S. Sugiyama, N. Shigemoto, N. Masaoka, S. Suetoh, H. Kawami, K. Miyaura and H. Hayashi, *Bull. Chem. Soc. Jpn.*, 1993, **66**, 1542.
12 H. Hayashi, S. Sugiyama, N. Masaoka and N. Shigemoto, *Ind. Eng. Chem. Res.*, 1995, **34**, 135.
13 S. Lomate, T. Bonnotte, S. Paul, F. Dumeignil and B. Katryniok, *J. Mol. Catal. A: Chem.*, 2013, **377**, 123.
14 I. E. Wachs and B. M. Weckhuysen, *Appl. Catal. A*, 1997, **157**, 67.
15 A. Khodakov, B. Olthof, A. T. Bell and E. Iglesia, *J. Catal.*, 1999, **181**, 205.
16 C. A. Carrero, R. Schloegl, I. E. Wachs and R. Schomaecker, *ACS Catal.*, 2014, **4**, 3357.
17 Q. Shi, Y. Li, E. Zhan, N. Ta and W. Shen, *CrystEngComm*, 2015, **17**, 3376.
18 M. Inomata, K. Mori, A. Miyamoto, T. Ui and Y. Murakami, *J. Phys. Chem.*, 1983, **87**, 754.
19 E. V. Ramos-Fernandez, N. J. Geels, N. R. Shiju and G. Rothenberg, *Green Chem.*, 2014, **16**, 3358.
20 X. Zhao, C. Zhang, C. Xu, H. Li, H. Huang, L. Song and X. Li, *Chem. Eng. J.*, 2016, **296**, 217.
21 A. Chieregato, J. M. López Nieto and F. Cavani, *Coord. Chem. Rev.*, 2015, **301–302**, 3.
22 D. W. Kwon, S. M. Lee, J. M. Won and S. C. Hong, *J. Chem. Eng. Jpn.*, 2015, **48**, 463.
23 F. Cavani, E. Foresti, F. Trifiró and G. Busca, *J. Catal.*, 1987, **106**, 251.
24 P. Ji, X. Gao, X. Du, C. Zheng, Z. Luo and K. Cen, *Catal. Sci.Technol.*, 2016, **6**, 1187.
25 F. Blanco-Bonilla, S. Lopez-Pedrajas, D. Luna, J. M. Marinas and F. M. Bautista, *J. Mol. Catal. A: Chem.*, 2016, **416**, 105.
26 F. M. Bautista, J. M. Campelo, D. Luna, J. Luque and J. M. Marinas, *Appl. Catal. A*, 2007, **325**, 336.
27 C. Caro, K. Thirunavukkarasu, M. Anilkumar, N. R. Shiju and G. Rothenberg, *Adv. Synth. Catal.*, 2012, **354**, 1327.
28 K. V. Bineesh, D.-K. Kim, M.-I. L. Kim and D.-W. Park, *Appl. Clay Sci.*, 2011, **53**, 204.
29 D. Nitsche and C. Hess, *J. Phys. Chem. C*, 2016, **120**, 1025.
30 H. Tian, E. I. Ross and I. E. Wachs, *J. Phys. Chem. B.*, 2006, **110**, 9593.
31 X. Gao and I. E. Wachs, *J. Phys. Chem. B*, 2000, **104**, 1261.
32 E. V. Danilevich, G. Y. Popova, T. V. Andrushkevich, V. V. Kaichev, I. G. Danilova, Y. A. Chesalov, V. A. Rogov, V. I. Bukhtiyarov and V. N. Parmon, *Appl. Catal. A*, 2014, **475**, 98.
33 D. Srinivas, W. F. Hölderich, S. Kujath, M. H. Valkenberg, T. Raja, L. Saikia, R. Hinze and V. Ramaswamy, *J. Catal.*, 2008, **259**, 165.
34 D. W. Kwon, K. H. Park and S. C. Hong, *Appl. Catal. A*, 2015, **499**, 1.
35 J. Beckers and G. Rothenberg, *Dalton Trans.*, 2008, 6573.
36 P. Concepción, M. T. Navarro, T. Blasco, J. M. López Nieto, B. Panzacchi and F. Rey, *Catal. Today*, 2004, **96**, 179.
37 M. V. Martínez-Huerta, X. Gao, H. Tian, I. E. Wachs, J. L. G. Fierro and M. A. Bañares, *Catal. Today*, 2006, **118**, 279.
38 Z. Li, K. Su, B. Cheng, D. Shen and Y. Zhou, *Catal. Lett.*, 2010, **135**, 135.
39 B. Schimmoeller, H. Schulz, A. Ritter, A. Reitzmann, B. Kraushaar-Czametzki, A. Baiker and S. E. Pratsinis, *J. Catal.*, 2008, **256**, 74.
40 D. W. Kwon, S. M. Lee and S. C. Hong, *Appl. Catal. A*, 2015, **505**, 557.
41 K. Sivaranjani, A. Verma and C. S. Gopinath, *Green Chem.*, 2012, **14**, 461.
42 H. Zhao, S. Bennici, J. Shen and A. Auroux, *Appl. Catal. A*, 2009, **356**, 121.
43 A. P. Amrute, C. Mondelli, M. Moser, G. Novell-Leruth, N. López, D. Rosenthal, R. Farra, M. E. Schuster, D. Teschner, T. Schmidt and J. Pérez-Ramírez, *J. Catal.*, 2012, **286**, 287.
44 J. Zhang, Y. Zhao, M. Pan, X. Feng, W. Ji and C.-T. Au, *ACS Catalysis*, 2010, **1**, 32.
45 M. Gallastegi-Villa, A. Aranzabal, Z. Boukha, J. A. González-Marcos, J. R. González-Velasco, M. V. Martínez-Huerta and M. A. Bañares, *Catal. Today*, 2015, **254**, 2.
46 Q. Wang and R. J. Madix, *Surf. Sci.*, 2002, **496**, 51.
47 G. Deo and I. E. Wachs, *J. Catal.*, 1994, **146**, 323.
48 I. E. Wachs and B. M. Weckhuysen, *Appl. Catal. A*, 1997, **157**, 67.
49 I. E. Wachs, J.-M. Jehng, G. Deo, B. M. Weckhuysen, V. V. Guliants and J. B. Benziger, *Catal. Today*, 1996, **32**, 47.

View Article Online
DOI: 10.1039/C7CY02309J

50 I. E. Wachs, *Dalton Trans.*, 2013, **42**, 11762.
51 T. Blasco and J. M. L. Nieto, *Appl. Catal. A*, 1997, **157**, 117.
52 I. E. Wachs, J.-M. Jehng, G. Deo, B. M. Weckhuysen, V. V. Guliants, J. B. Benziger and S. Sundaresan, *J. Catal.*, 1997, **170**, 75.
53 J. Datka, A. M. Turek, J. M. Jehng and I. E. Wachs, *J. Catal.*, 1992, **135**, 186.
54 S. Velu, M. P. Kapoor, S. Inagaki and K. Suzuki, *Appl. Catal. A*, 2003, **245**, 317.
55 Y.-K. Chen, Y.-F. Lin, Z.-W. Peng and J.-L. Lin, *J. Phys. Chem. C*, 2010, **114**, 17720.
56 G. Cassanas, M. Morssli, E. Fabrègue and L. Bardet, *J. Raman Spectrosc.*, 1991, **22**, 409.
57 B. Wen, Y. Li, C. Chen, W. Ma and J. Zhao, *Chem. Eur. J.*, 2010, **16**, 11859.
58 K. Krauß, A. Drochner, M. Fehlings, J. Kunert and H. Vogel, *J. Mol. Catal. A: Chem.*, 2000, **162**, 413.
59 A. Chieregato, C. Bandinelli, P. Concepción, M. D. Soriano, F. Puzzo, F. Basile, F. Cavani and J. M. L. Nieto, *ChemSusChem*, 2017, **10**, 234.
60 V. V. Kaichev, Y. A. Chesalov, A. A. Saraev, A. Y. Klyushin, A. Knop-Gericke, T. V. Andrushkevich and V. I. Bukhtiyarov, *J. Catal.*, 2016, **338**, 82.
61 F. Folco, J. Velasquez Ochoa, F. Cavani, L. Ott and M. Janssen, *Catal. Sci.Technol.*, 2017, **7**, 200.
62 K. Hanai, A. Kuwae, K.-K. Kunimoto and S.-I. Kitoh, *Eur. J. Chem.*, 2014, **5**, 305.
63 O. Seiferth, K. Wolter, B. Dillmann, G. Klivenyi, H. J. Freund, D. Scarano and A. Zecchina, *Surf. Sci.*, 1999, **421**, 176.
64 S. C. A. Sousa and A. C. Fernandes, *Coord. Chem. Rev.*, 2015, **284**, 67.
65 Y.-D. Ding, G. Song, X. Zhu, R. Chen and Q. Liao, *RSC Adv.*, 2015, **5**, 30929.
66 N. A. Davshan, A. L. Kustov, O. P. Tkachenko, L. M. Kustov and C. H. Kim, *ChemCatChem*, 2014, **6**, 1990.
67 J. Li, Z. Zhang, Z. Tian, X. Zhou, Z. Zheng, Y. Ma and Y. Qu, *J. Mater. Chem. A*, 2014, **2**, 16459.

View Article Online
DOI: 10.1039/C7CY02309J